Higher-order source-wavefield reconstruction for reverse-time migration from stored values in a boundary strip just one point wide

Mulder, Wim

DOI
10.3997/2214-4609.201700681

Publication date
2017

Document Version
Accepted author manuscript

Published in
79th EAGE Conference & Exhibition 2017

Th P1 14

Higher-Order Source-Wavefield Reconstruction for Reverse-Time Migration From Stored Values in a Boundary Strip Just One Point Wide

W.A. Mulder, (Shell Global Solutions International BV and Delft University of Technology)

Summary

Storage of the source wavefield during reverse-time migration and full-waveform inversion can be avoided by reconstructing that wavefield during reverse-time stepping along with the receiver wavefield. With absorbing boundary conditions, this requires the final states of the source wavefield and a strip of boundary values at all times. The width of the stored boundary strip, positioned in between the interior domain and the absorbing boundary region, usually equals about half that of the finite-difference stencil. The required storage in 3D with high frequencies can still adversely affect computational efficiency, despite the huge reduction in data volume compared to storing the source wavefields at all or appropriately subsampled time steps.

A method is proposed that requires a boundary strip with a width of just one point. Stored boundary values over time enable the computation of the second and higher even derivatives normal to the boundary, which together with extrapolation from the interior provides stability and accuracy. Numerical tests show that the use of only the boundary values provides at most fourth-order accuracy for the reconstruction error in the source wavefield. With the higher even normal derivatives, higher orders can be reached as is demonstrated by examples up to order 26.

Introduction

Subsurface imaging from seismic data with reverse-time migration (RTM) or full-waveform inversion (FWI) requires the correlation of forward-propagated source wavefields and backward-propagated reverse-time receiver wavefields. 3-D RTM typically employs higher frequencies than FWI and storage of source wavefields on disk or solid-state drives or even main memory may lead to performance bottlenecks, in particular on many-core or GPU hardware. Migration in the frequency domain avoids the storage problem and outperforms migration in the time domain in 2D, but not yet in 3D (Amestoy et al., 2016). For 3D applications, there are several ways to reduce or circumvent the storage of the source wavefields. Data compression with sub-sampling or with wavelet or Fourier transforms is one approach (Araya-Polo et al., 2011; Knibbe et al., 2014). Check-pointing, storing the wavefield at selected times to recompute the wavefields in small time intervals when needed for correlation with the reverse-time computations, is another (Griewank, 1992; Symes, 2007). Reliance on the time-reversibility of the wave equation requires no storage at all with Dirichlet or Neumann boundary conditions, at the expense of recomputing the source wavefield in reverse time, along with the receiver wavefield. Clapp (2009) proposed reflecting boundaries with nearby random velocity perturbations that generate incoherent backscatter. Time reversal of the source wavefield is exact and the backscattered waves do not constructively interfere into a subsurface image, although some noise will remain. With absorbing boundaries, time reversal for source-wavefield reconstruction only works if a strip of boundary values just inside the absorbing region with a width of about half the finite-difference stencil is stored (Dussaud et al., 2008, a.o.). Feng and Wang (2012) accomplished a width of one point by lowering the order of the scheme towards the boundary strip, leading to some loss of accuracy. Tan and Huang (2014) maintain accuracy using the Lax-Wendroff (1960) idea to translate temporal into spatial derivatives via the wave equation on the boundary together with extrapolation from the interior. They only need a strip of one point wide for lower-order schemes. Stability with higher orders requires additional layers. Liu et al. (2015) apply the same idea to find the second spatial derivative in the normal direction on the boundary. They combine it with extrapolation from the interior and with the partial action of a dedicated discrete second-derivative operator on the exterior values, stored during the forward computations in a buffer of the same storage size as a one-point-wide strip. Here, I propose an alternative method that, in principle, should make subsampling in time straightforward. 2-D tests reveal its stability properties as well as convergence behaviour in terms of the error in the the reconstructed source wavefield as a function of grid spacing.

Method

To explain the idea, the constant-density acoustic wave equation is considered:

$$\frac{1}{c^2}\frac{\partial^2 p}{\partial t^2} = f + \frac{\partial^2 p}{\partial x^2} + \frac{\partial^2 p}{\partial y^2} + \frac{\partial^2 p}{\partial z^2}. \tag{1}$$

The pressure $p(t,\mathbf{x})$ depends on time t and position $\mathbf{x} = (x,y,z)$. The velocity is denoted by $c(\mathbf{x})$ and the source term by $f(t,\mathbf{x})$. An equidistant grid has points $x = x_0 + \ell h_x$ for $\ell = 0,\ldots,N_x - 1$, and similarly for y and z. Standard second-order time stepping is combined with higher-order second-derivative operators in space that have a stencil width of $M+1$ points in each coordinate. Expressions for the weights and stability limits can be found elsewhere (Fornberg, 1988; Zhebel et al., 2014). In the context of reverse-time migration, all boundaries are assumed to be absorbing. To that end, the domain is enlarged on all sides.

Consider just one boundary, for instance the lower one at $x = x_0$. The computational domain is enlarged. Around x_0, we introduce $x_{\min} < x_a < x_b < x_0$. The absorbing boundary covers the interval $[x_{\min}, x_a]$. For the tests in the next section, sponge boundaries (Cerjan et al., 1985) are applied, which are easy to code up but not recommended for serious applications. Solution values located at x_b are stored during the forward simulation. The velocity is extended outside its original domain by constant extrapolation, making it constant along $x \le x_0$, but not necessarily in the boundary plane, spanned by y and z at $x = x_b$. For the reverse-time reconstruction of the source wavefield, we can consider the stored boundary values at x_b together with extrapolation from the interior to produce pressure values at positions $x_\ell < x_b$ needed for the finite differencing in x, or, equivalently, we can apply a one-sided difference scheme. Unfortunately,

that approach quickly leads to an unstable scheme when increasing the spatial order. Stability can be recovered by computing the even spatial derivatives in the direction normal to the boundary from stored pressure boundary values, $p(t,x_b,y,z)$, using the wave equation and assuming sufficient smoothness of the solution:

$$\frac{\partial^{2k} p}{\partial x^{2k}}(t,x_b,y,z) = \left[\frac{1}{c^2}\frac{\partial^2}{\partial t^2} - \frac{\partial^2}{\partial y^2} - \frac{\partial^2}{\partial z^2}\right]^k p(t,x_b,y,z), \quad k = 0,1,...,M_t. \tag{2}$$

The k-th power of the differential operator means it should be applied k times. At fixed y and z, these M_t+1 values for the even normal derivatives at x_b together with an additional n_i additional interior points, located at $x = x_b + jh_x$ ($j = 1,\ldots,n_i$), define an interpolating polynomial of the form $p(x) = \sum_k b_k (x-x_b)^k/k!$ with M_t+1 coefficients $b_0, b_2, \ldots, b_{2M_t}$ and n_i coefficients $b_1, b_3, \ldots, b_{2M_t-1}$ together with $b_{2M_t+1}, b_{2M_t+2}, \ldots$. Note that if $2n_i - 1 < 2M_t - 1$ or $n_i < M_t$, there are not enough interior points to define all derivatives up to $2M_t$. A natural choice for n_i is to match the stencil width of the discrete spatial operator, implying $n_i + M_t + 1 = M + 1$. The polynomial $p(x)$ determines extrapolated solution values at points outside the domain, at $x = x_b + jh_x$ with $j = -(\frac{1}{2}M-1), \ldots, -1$, providing sufficient input to evaluate the standard discrete Laplace operator, requiring $\frac{1}{2}M$ neighbours, at the interior points $x = x_b + jh_x$, with $j = 1,\ldots,\frac{1}{2}M-1$. The reverse-time computation now only requires values for $x \geq x_b$, but some extra points are needed in t, y, and z to be able to evaluate the derivatives in equation (2). The same approach should be taken on the other boundary planes.

The combination of extrapolation and standard finite differencing produces a modified, one-sided finite-difference scheme for interior points near the boundary. For $M_t = 0$, such a scheme is known to become unstable at higher orders. Increasing M_t will recover stability as will be demonstrated in the next section. Note that storing $\frac{1}{2}M$ boundary points yields an exact reconstruction of the source wavefield, but still involves a fair amount of data in 3D for higher orders.

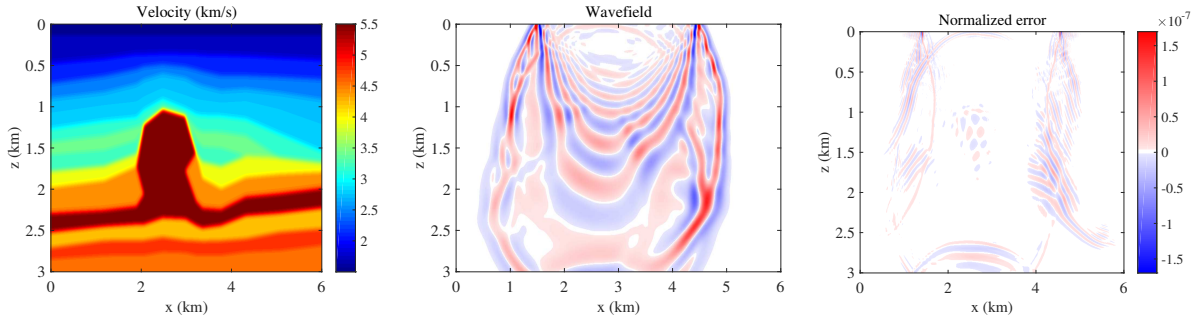

Figure 1 *(a) 2-D velocity model, (b) source wavefield at* 1 *s and (c) its normalized reconstruction error at the same time, for a scheme with* $M = 8$, $M_t = 1$, *and* $n_i = 7$ *and a* 5*-m grid spacing.*

Results

A series of 2-D tests were performed to study the stability and convergence of the proposed scheme for a range of spatial orders, M, and using only one boundary value with $M_t = 0$, meaning just the pressure value, or using the second ($M_t = 1$) and higher ($M_t > 1$) even normal derivatives computed from the stored values on the boundaries.

Table 1 *Values of* n_i *as a function of* M_t *for which the method appeared to be unstable in the 2D test and the affected orders* M.

M_t	0	1	2	3	4	5
$n_i \geq$	6	9	12	15	18	21
$M \geq$	6	10	14	18	22	26

Figure 1a displays the velocity model for the numerical tests. The source at $x_s = 3000$ m and $z_s = 0$ m has a 15-Hz Ricker wavelet that peaks at zero time. The forward source wavefield is propagated to $t_{\max} = 2$ s at 90% of the maximum time step. Then, the time-reversed computation starts back to a time of 1 s. The resulting wavefield is compared to a snapshot at the same time, saved for that purpose during the forward modelling. Figure 1b shows an example of the forward wavefield at 1 s for a set of parameters and 1c its normalized reconstruction error, defined as the difference between the reconstructed and true source wavefield at the same time, divided by the maximum amplitude of the true source wavefield.

Table 1 lists parameters for which the method became unstable. The suggested trend is instability for $n_i \geq 6+3M_t$. Assuming that the boundary order is at most the interior spatial order or less, the instability affects orders $M \geq n_i + M_t = 6+4M_t$.

Table 2 *Maximum and root-mean-square errors in the reconstructed source wavefield, divided by its maximum amplitude over the domain, as a function of grid spacing $h_x = h_z = h$ for a finite-difference scheme of order M, using extrapolation with even normal derivatives up to $2M_t$ on the boundary and n_i interior points. Convergence behaves as h^q with order q.*

			maximum error				root-mean-square error			
M	M_t	n_i	$h = 20\,\mathrm{m}$	$10\,\mathrm{m}$	$5\,\mathrm{m}$	q	$h = 20\,\mathrm{m}$	$10\,\mathrm{m}$	$5\,\mathrm{m}$	q
2	0	0	–	–	–	–	–	–	–	–
4	0	0	$3.6\,10^{-2}$	$1.4\,10^{-2}$	$7.5\,10^{-3}$	1.1	$2.3\,10^{-3}$	$9.9\,10^{-4}$	$7.0\,10^{-4}$	0.9
	0	1	$3.2\,10^{-2}$	$7.2\,10^{-3}$	$1.7\,10^{-3}$	2.1	$1.8\,10^{-3}$	$3.7\,10^{-4}$	$1.1\,10^{-4}$	2.0
	0	2	$3.4\,10^{-2}$	$3.8\,10^{-3}$	$6.5\,10^{-4}$	2.9	$1.8\,10^{-3}$	$2.0\,10^{-4}$	$3.6\,10^{-5}$	2.8
	0	3	$4.3\,10^{-2}$	$2.7\,10^{-3}$	$2.2\,10^{-4}$	3.8	$2.3\,10^{-3}$	$1.3\,10^{-4}$	$1.1\,10^{-5}$	3.9
4	0	4	$7.1\,10^{-2}$	$2.1\,10^{-3}$	$1.5\,10^{-4}$	4.4	$3.7\,10^{-3}$	$9.7\,10^{-5}$	$4.3\,10^{-6}$	4.9
	0	5	0.17	$1.7\,10^{-3}$	$5.1\,10^{-5}$	5.8	$9.7\,10^{-3}$	$7.8\,10^{-5}$	$1.7\,10^{-6}$	6.2
4	1	0	$3.2\,10^{-2}$	$1.3\,10^{-2}$	$7.2\,10^{-3}$	1.1	$2.1\,10^{-3}$	$9.7\,10^{-4}$	$6.9\,10^{-4}$	0.8
	1	1,2	$2.7\,10^{-3}$	$1.8\,10^{-4}$	$1.2\,10^{-5}$	3.9	$1.6\,10^{-4}$	$9.1\,10^{-6}$	$7.3\,10^{-7}$	3.9
	1	3	$3.5\,10^{-3}$	$1.4\,10^{-4}$	$9.3\,10^{-6}$	4.3	$2.1\,10^{-4}$	$6.5\,10^{-6}$	$3.0\,10^{-7}$	4.7
	1	4	$4.6\,10^{-3}$	$1.1\,10^{-4}$	$3.3\,10^{-6}$	5.2	$3.0\,10^{-4}$	$5.1\,10^{-6}$	$1.1\,10^{-7}$	5.7
4	2	1,2	$7.3\,10^{-4}$	$1.7\,10^{-5}$	$4.9\,10^{-7}$	5.3	$4.7\,10^{-5}$	$7.5\,10^{-7}$	$1.6\,10^{-8}$	5.7
6	0	5	0.14	$1.6\,10^{-3}$	$4.3\,10^{-5}$	5.8	$7.6\,10^{-3}$	$6.8\,10^{-5}$	$1.3\,10^{-6}$	6.3
6	1	5	$2.9\,10^{-3}$	$7.6\,10^{-5}$	$1.2\,10^{-6}$	5.6	$1.6\,10^{-4}$	$3.2\,10^{-6}$	$4.2\,10^{-8}$	6.0
8	1	7	$8.8\,10^{-3}$	$4.0\,10^{-5}$	$1.7\,10^{-7}$	7.8	$5.1\,10^{-4}$	$1.7\,10^{-6}$	$3.4\,10^{-9}$	8.6
10	1	8	$1.5\,10^{-2}$	$2.9\,10^{-5}$	$6.4\,10^{-8}$	8.9	$1.1\,10^{-3}$	$1.3\,10^{-6}$	$1.7\,10^{-9}$	9.7
10	2	8	$9.4\,10^{-4}$	$2.5\,10^{-6}$	$2.5\,10^{-9}$	9.3	$5.5\,10^{-5}$	$1.2\,10^{-7}$	$4.9\,10^{-11}$	10
12	2	10	$2.2\,10^{-3}$	$1.1\,10^{-6}$		11	$1.6\,10^{-4}$	$5.1\,10^{-8}$		12
14	3	11	$4.3\,10^{-4}$	$1.1\,10^{-7}$			$2.7\,10^{-5}$	$5.2\,10^{-9}$		
16	3	13	$1.3\,10^{-3}$	$5.1\,10^{-8}$			$7.4\,10^{-5}$	$2.4\,10^{-9}$		
18	4	14	$3.5\,10^{-4}$	$1.2\,10^{-8}$			$1.7\,10^{-5}$	$4.1\,10^{-10}$		
20	4	16	$1.7\,10^{-3}$	$8.0\,10^{-9}$			$4.0\,10^{-5}$	$3.9\,10^{-10}$		
22	5	17	$5.2\,10^{-4}$	$1.9\,10^{-9}$			$1.1\,10^{-5}$	$9.1\,10^{-11}$		
24	5	19	$1.1\,10^{-3}$	$6.6\,10^{-9}$			$2.3\,10^{-5}$	$2.6\,10^{-10}$		
26	6	20	$1.5\,10^{-4}$	$1.5\,10^{-9}$			$4.2\,10^{-6}$	$6.0\,10^{-11}$		

Table 2 lists the measured maximum and root-mean-square difference between the reconstructed and stored source wavefields at 1 s, divided by that wavefield's maximum amplitude over the domain. With the second-order scheme ($M = 2$), one boundary point already suffices to recover the source wavefield within machine precision. For higher orders, various combinations of even spatial order M, up to $M_t + 1$ even normal boundary derivatives, and n_i interior points were considered. The choice $n_i < M_t$ is allowed but not sensible as there are not enough interior points to determine all odd derivatives up to degree $2M_t$. Choosing $n_i + M_t < M$ will lower and $n_i + M_t > M$ will raise the order of the boundary scheme. The convergence behaviour of the normalized reconstruction error, ε, as a function of grid spacing h, is $\varepsilon \propto h^q$, where the power q can be estimated by a linear fit to a log-log plot.

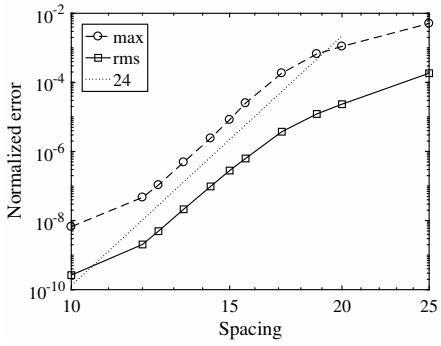

Table 3 *Maximum and root-mean-square error as a function of grid spacing for order $M = 24$ with $M_t = 5$ and $n_i = 19$, showing how small the interval is where the expected error slope marked by the dotted line is attained.*

To illustrate the effect of the parameters, Table 2 explores a lengthy range of options for interior order $M = 4$. The natural choice is $M_t = 0$ and $n_i = M - M_t = 4$. For other choices, the estimated power q becomes larger or smaller. Note that measuring q from the maximum error produces more erratic values than from the root-mean-square error. The results for

$M_t = 1$ and $n_i = 2$ are the same as those for $n_i = 1$, because for $n_i = 2$, the extrapolation weight for the interior point farthest from the boundary happens to be zero. The same is true with $M = 4$ and $M_t = 2$. For higher orders, only a subset of the results is presented, up to order $M = 26$. At higher orders, it becomes more difficult to estimate the scheme's order of accuracy, because of the smaller range of grid spacings where convergence can be estimated, as illustrated in Figure 3 for order $M = 24$. If the spacing is too large, the region of asymptotic convergence is not yet reached, whereas for too small a spacing, round-off errors start to dominate. For that reason, Table 2 lists estimated powers only up to $M = 12$.

Conclusions

The computation of even spatial derivatives normal to boundary from stored boundary values with a width of just one point in combination with extrapolation from interior points enables the reconstruction of a source wavefield during reverse time stepping with improved accuracy. Whereas only fourth-order accuracy is observed when only the boundary values are used, higher orders are obtained if the second and higher even normal derivatives are determined from the stored boundary values. Stability and accuracy were tested up to order 26 for a 2-D example. Generalization to 3D and to subsampling in time should be straightforward.

Acknowledgement. The author is grateful to Eric Duveneck for his comments on the manuscript.

References

Amestoy, P., Brossier, R., Buttari, A., L'Excellent, J.Y., Mary, T., Métivier, L., Miniussi, A. and Operto, S. [2016] Fast 3D frequency-domain full-waveform inversion with a parallel block low-rank multifrontal direct solver: Application to OBC data from the North Sea. *Geophysics*, **81**(6), R363–R383.

Araya-Polo, M., Cabezas, J., Hanzich, M., Pericas, M., Rubio, F., Gelado, I., Shafiq, M., Morancho, E., Navarro, N., Ayguade, E., Cela, J.M. and Valero, M. [2011] Assessing Accelerator-Based HPC Reverse Time Migration. *IEEE Transactions on Parallel and Distributed Systems*, **22**(1), 147–162.

Cerjan, C., Kosloff, D., Kosloff, R. and Reshef, M. [1985] A nonreflecting boundary condition for discrete acoustic and elastic wave equations. *Geophysics*, **50**(4), 705–708.

Clapp, R.G. [2009] Reverse time migration with random boundaries. In: *SEG Technical Program Expanded Abstracts 2009*. 2809–2813.

Dussaud, E., Symes, W.W., Williamson, P., Lemaistre, L., Singer, P., Denel, B. and Cherrett, A. [2008] Computational strategies for reverse-time migration. In: *SEG Technical Program Expanded Abstracts 2008*. 2267–2271.

Feng, B. and Wang, H. [2012] Reverse time migration with source wavefield reconstruction strategy. *Journal of Geophysics and Engineering*, **9**(1), 69.

Fornberg, B. [1988] Generation of finite difference formulas on arbitrarily spaced grids. *Mathematics of Computation*, **51**, 699–706.

Griewank, A. [1992] Achieving logarithmic growth of temporal and spatial complexity in reverse automatic differentiation. *Optimization Methods and Software*, **1**(1), 35–54.

Knibbe, H., Mulder, W.A., Oosterlee, C.W. and Vuik, C. [2014] Closing the performance gap between an iterative frequency-domain solver and an explicit time-domain scheme for 3D migration on parallel architectures. *Geophysics*, **79**(2), S47–S61.

Lax, P. and Wendroff, B. [1960] Systems of conservation laws. *Communications on Pure and Applied Mathematics*, **31**(2), 217–237.

Liu, S., Li, X., Wang, W. and Zhu, T. [2015] Source wavefield reconstruction using a linear combination of the boundary wavefield in reverse time migration. *Geophysics*, **80**(6), S203–S212.

Symes, W.W. [2007] Reverse time migration with optimal checkpointing. *Geophysics*, **72**(5), 213–221.

Tan, S. and Huang, L. [2014] Reducing the computer memory requirement for 3D reverse-time migration with a boundary-wavefield extrapolation method. *Geophysics*, **79**(5), S185–S194.

Zhebel, E., Minisini, S., Kononov, A. and Mulder, W.A. [2014] A comparison of continuous mass-lumped finite elements with finite differences for 3-D wave propagation. *Geophysical Prospecting*, **62**, 1111–1125.